Self organization of magnetic nanoparticles: A polarized grazing incidence small angle neutron scattering and grazing incidence small angle x-ray scattering study

Katharina Theis-Bröhl, Durgamadhab Mishra, Boris P. Toperverg, Hartmut Zabel, Britta Vogel, Anna Regtmeier, and Andreas Hütten

Citation: Journal of Applied Physics **110**, 102207 (2011); doi: 10.1063/1.3661654
View online: http://dx.doi.org/10.1063/1.3661654
View Table of Contents: http://scitation.aip.org/content/aip/journal/jap/110/10?ver=pdfcov
Published by the AIP Publishing

Self organization of magnetic nanoparticles: A polarized grazing incidence small angle neutron scattering and grazing incidence small angle x-ray scattering study

Katharina Theis-Bröhl,[1,a)] Durgamadhab Mishra,[2] Boris P. Toperverg,[2,3] Hartmut Zabel,[2] Britta Vogel,[4] Anna Regtmeier,[4] and Andreas Hütten[4]
[1]*University of Applied Sciences Bremerhaven, An der Karlstadt 8, D-27568 Bremerhaven, Germany*
[2]*Institute for Solid State Physics, Department of Physics, Ruhr-University Bochum, D-44780 Bochum, Germany*
[3]*Petersburg Nuclear Physics Institute, 188300 Gatchina, Russia*
[4]*Thin films and nanostructures, Faculty of Physics, Bielefeld University, D-33615 Bielefeld, Germany*

(Received 15 October 2010; accepted 17 February 2011; published online 30 November 2011)

Cobalt and magnetite nanoparticles were studied with small-angle x-ray and neutron scattering methods under grazing incidence for analyzing their structural and magnetic correlation on silicon substrates. The Co nanoparticles are in the ferromagnetic state while the iron oxide nanoparticles are superparamagnetic at room temperature. After spin-coating the iron oxide particles with a diameter of 20 nm and a very narrow size distribution of only 6% show very nice self-ordering on silicon substrates with nearly perfect six-fold symmetry as can be derived from scanning electron microscopy (SEM) images and from grazing incidence small angle x-ray scattering results. In contrast the dropcasted cobalt nanoparticles show a much higher roughness and less ordering. The corresponding SEM images and grazing incidence small angle neutron scattering maps with polarization of the incident beam reveal less pronounced structural and magnetic correlation. © *2011 American Institute of Physics*. [doi:10.1063/1.3661654]

I. INTRODUCTION

Magnetic nanoparticles exhibit attractive properties for potential use in different fields such as for biomedical and biotechnology applications,[1–3] for high-density magnetic memory systems, or for spintronic applications.[4,5] Such nanoparticles are mostly based on FeO or Fe_3O_4 iron compounds.[6,7] For the future, however, they could be substituted by nanoparticles of materials with a higher saturation magnetization such as Co, CoFe, or FePt (Refs. 8–11) nanoparticles. Besides biocompability, for applications nanoparticles should also exhibit well-defined magnetic properties depending on shape, size, and composition. In particular for magnetic memory and spintronic applications well-ordered monolayers are required. Furthermore, often agglomeration of the ferromagnetic nanoparticles is encountered, which hampers self-assembled ordering on substrates. Self-organization into ordered arrays very much depends on their size, magnetization, ambient medium, and other parameters[12,13] and is subject of current studies. Direct imaging methods such as transmission electron microscopy (TEM) and scanning electron microscopy (SEM) provide important information about shape, distribution and on lateral ordering of nanoparticle complexes deposited onto substrates.[14,15] However, these methods are restricted to the image of the top layer and do not provide sufficient depth sensitivity to record short and long range correlations in three dimensions. This is particularly important, if nanoparticles form layered or crystal-like 3 D structures. Furthermore, these methods are not sensitive to the magnetic order and magnetic correlations.

We employed scattering methods for getting insight into the in- and out-of-plane ordering of magnetic nanoparticles on a silicon substrate. We combined grazing incidence small angle neutron scattering (GISANS) with polarized incident beam (PGISANS) with polarized neutron reflectometry (PNR) in order to gain simultaneous access to information on the structural arrangement over a broad range of length scales in the lateral direction as well as in the transverse direction. In addition, non-resonant grazing incidence small angle x-ray scattering (GISAXS) was performed for structural analysis of nanoparticle arrays.

II. SAMPLE PREPARATION AND CHARACTERIZATION

For the assembly of nanoparticles into mono- and multilayers on a substrate several methods are available. The most simple one is dropcasting of a colloidal solution of nanoparticles onto a substrate and subsequent evaporation of the solvent. By repeating this dropping procedure three-dimensional assemblies can be achieved. Figure 1(a) pictures a multilayer structure of 13.5 nm oleyl amine stabilized Co nanoparticles, which are drop-deposited on a SiO_2 substrate. Since the evaporation-induced assembly is a complex, non-equilibrium process requiring precise control of numerous factors, high surface roughnesses and a lack of ordering may result.[21]

Another possibility for the preparation of wide range assemblies is the spin-coating process that allows for uniform distribution of the nanoparticles and controllable density of the layers. The spin coating method was used to prepare wide areas of ordered mono- and multilayer assemblies of FeO-nanoparticles, as shown in Figs. 1(b) and 1(c), respectively. Compared to the dropcasted sample the surface roughness of

a)Electronic mail: k.theis-broehl@rub.de.

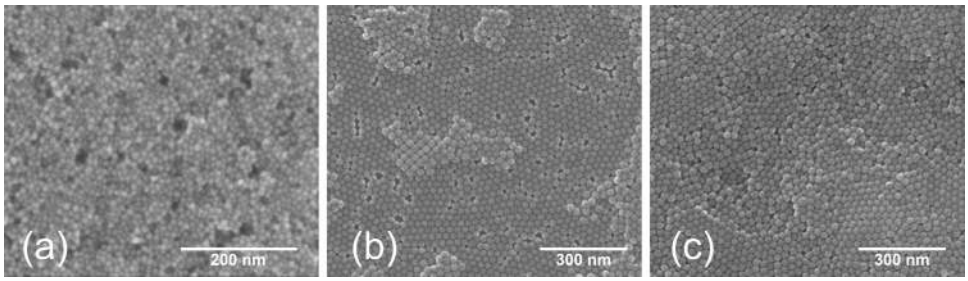

FIG. 1. SEM images of the top surface of self assembled spherical nanoparticles on substrates. (a) 3 monolayers of (13.5 ± 1.0) nm Co nanoparticles, self-assembled by repeated drop coating; (b) monolayer of 20 nm FeO nanoparticles and self assembled by spin coating; and (c) 4 monolayers of 20 nm FeO nanoparticles self assembled by spin coating.

the 20 nm oleic acid stabilized FeO-nanoparticles is clearly reduced. This results in a better reflectivity that is necessary for the PNR measurements. The organization process of magnetic nanoparticles on a surface is a complex interplay between interparticle interactions and external forces that is still not totally understood. For example because of their magnetism compared to FeO nanoparticles one of the future challenges is to achieve highly-ordered wide range mono- and multilayer Co and FeCo-nanoparticle assemblies.[22] Figure 1(d) shows a monolayer of 7 nm FeCo-nanoparticles that are stabilized with a mixture of oleyl amino and oleic acid. Comparable to the results of FeO nanoparticles here also only a very small number of lattice distortions can be found that may result in a reduced surface roughness of a multilayer assembly.

III. SCATTERING METHODS

Neutrons, deeply penetrating into the film are either specularly reflected from the mean optical potential or scattered in off-specular directions due to fluctuations of the potential within the coherence ellipsoid. At grazing incidence this ellipsoid is highly anisotropic.[16,17] Its long axis (x-axis) is parallel to the projection of the incident beam onto the surface. At grazing incidence it may reach an extension up to 100 μm. The two other axes of the ellipsoid are within the range of only 10–100 nm. One of them (the z-axis) is normal to the surface while the other one (the y-axis) is within the surface plane and normal to the reflection plane. Traditionally, in reflectometry and in particular in PNR, the resolution along the y-axis is almost totally relaxed so that the scattered intensity containing specular reflection and off-specular scattering integrated over the y-direction is measured as a function of incident and scattered wave vector projections normal to the surface. In contrast, GISANS, or better PGISANS, requires a point-like beam collimation providing almost equal resolution in z- and y-directions, comparable with that of PNR along only the z-axis. Therefore both, NR and GISANS, probe comparable out-of-plane length scales but different in-plane length scales. Thus, on first sight it appears that PGISANS provides more complete information than PNR. This, however, may only be true if the GISANS signal is recorded over a range of incident wave vectors as broad, as is usual in reflectometry. In practice, the GISANS signal is usually recorded at very few incident wave vectors providing some fragments of information on the nano-system. Reflectometry adds some essential fragments of missing information, in particular, on the depth profile of the mean optical potential averaged over the large coherence length in x-direction, as well as on long range correlations of fluctuations around this mean value. PNR data are valuable not only in view of completeness of information on nano-system arrangements, but are absolutely required, as we shall see, for a quantitative theoretical description and interpretation of data taken with GISANS.

IV. PNR RESULTS ON CO NANOPARTICLES

The PNR measurements were carried out on the reflectometer ADAM (Refs. 18 and 19) at the Institut Laue Langevin (Grenoble, France). The incident beam with a fixed neutron wavelength of $\lambda = 0.441$ nm was collimated down to 0.25 mrad, and the polarization of the incident beam was determined to be around 98% and the efficiency of polarization analysis of the final spin states was about 90%. Figure 2 shows the non-spin flip (NSF), $R^{\pm\pm}$, and spin-flip (SF), $R^{\pm\mp}$, specular reflectivities from a sample with 18 layers of Co nanoparticles with a diameter of (13.5 ± 1.0) nm, measured in saturation (the saturation field $H_S \approx 200$ mT was determined from the hysteresis, measured via alternating gradient magnetometry). The NSF reflectivities probe the magnetization projection onto the applied field guiding the neutron polarization, while the SF reflectivities are sensitive to the magnetization components perpendicular to the field direction. However, in saturation the SF intensity visible in Fig. 2, can totally be attributed to the non-perfect polarization efficiency of the spin analyzer. Therefore, we conclude that the magnetization of the Co nanoparticles is well aligned with the external field and the NSF reflection curves $R^{\pm\pm}$ record the depth profiles of either the sum or the difference of the nuclear and magnetic scattering length density (SLD). On the reflectivity curves no trace of Bragg peaks as expected

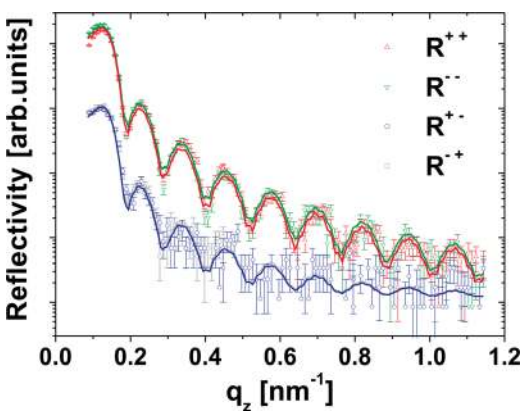

FIG. 2. (Color online) PNR data taken from 18 layers of Co nanoparticles with a diameter of (13.5 ± 1.0) nm deposited on a Si substrate. Data are taken in a high field as to magnetically saturate the sample. The solid lines represent fits to the data points.

for the periodic layered superstructure of the film is detected, while well resolved Kiessig fringes result from a 50 nm thick SiO_2 layer on the substrate.

The specular PNR data were fitted to a theoretical model by using a least squares routine allowing simultaneous evaluation of all four measured reflectivities in one cycle.[16,23] The fitting reveals no tendency of nanoparticle layering. The fitted nuclear and magnetic SLD profiles are depicted in Fig. 3. For comparison nuclear and magnetic SLD values for Co, oleyl amine and CoO are indicated in Fig. 3 with dashed lines. The magnetic contribution to PNR is related to a (298 ± 7) nm thick continuous layer. The best fit was achieved for a magnetic SLD of the film of $Np = (0.75 \pm 0.06) \times 10^{-6}$ Å^{-2} and a nuclear one of $Nb = (0.36 \pm 0.08) \times 10^{-6}$ Å^{-2}. The fit (Fig. 2) also shows that the magnetization of the Co nanoparticles is completely aligned with the applied field, i.e., the sample is in saturation. This allows one to immediately determine the Co content of 18% by using the theoretical value for Co $Np^{th}_{Co} = 4.27 \times 10^{-6}$ Å^{-2}, a center-to-center inter-particle distance of 16.5 nm as also determined from the PGISANS measurements (see below) and assuming a nearly fcc packing of the nanoparticles.[20] For a thinner nanoparticle film with only 3 layers of the same Co nanopartices, the fitting procedure yields a thickness of the nanoparticle layer of (49 ± 3) nm and very similar SLDs as for the 18 layer sample. From the reflectivity data it can also be inferred that the Co nanoparticles have a diameter of 13.5 nm. This is in good agreement with the (13.5 ± 1.0) nm derived from TEM-analysis.

Note, that specular PNR resolves the SLD depth profile averaged over the lateral projection of the coherence length $l_c \sim 100\,\mu$m. PNR can reveal layering via Bragg reflections only if the SLD laterally averaged over scales larger than l_c varies periodically. Therefore, we conclude that layering of the nanoparticles is not extended over large length scales. It, however, cannot be excluded that fluctuations exist within domain-like areas that are much smaller than l_c. This hypothesis was examined with small angle neutron scattering probing lateral and transverse scales down to 100 nm.

V. PGISANS RESULTS ON CO NANOPARTICLES

The PGISANS experiments were performed on the small-angle machine D22 (Institut Laue Langevin (Grenoble, France)) in polarized mode. The collimation base of the incident beam with $\lambda \approx 1.0$ nm and $\Delta\lambda/\lambda = 10\%$ was set to 5.6 m and the detector distance was chosen to be 6 m in order to be optimized to catch the SANS from the 13,46 nm nanoparticles (as determined previously via TEM) at $q \approx 0.5$ nm^{-1}. An additional slit of 1×10 mm^2 was placed in front of the sample for background reduction. A horizontal electromagnet with the field oriented along the beam provided the desired magnetic fields. Then polarization of the incident beam was determined to 91% in a magnetic field of $H = 180$ mT and to around 84% at $H = 70$ mT. No polarization analysis of the scattered beam was applied.

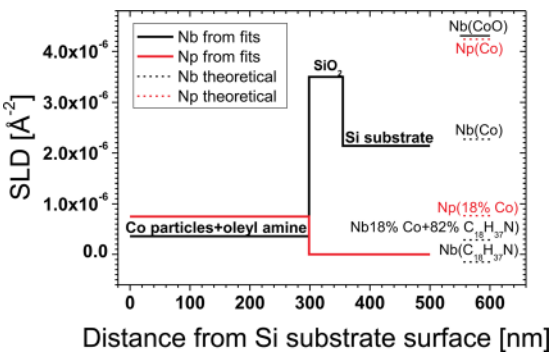

FIG. 3. (Color online) Profile of nuclear and magnetic scattering length densities plotted as a function of distance from the sample surface. For comparison nuclear (Nb) and magnetic (Np) SLDs for Co, CoO, and oleyl amine ($C_{18}H_{37}N$) are shown.

Figure 4 shows data collected at an incident angle of 1.1°, well above the critical angle of total reflection. The sample was measured in magnetic fields of 110 mT (Ref. 24) and without field. The panels in the left column of Fig. 4 show the difference $I^+ - I^-$ between the intensity distributions $I^{\pm}(q_y, q_z')$ (Ref. 25) for Co nanoparticle films with 18 layers (top left) and 3 layers (bottom left). The panels in the right column illustrate the scattered intensity distribution for the sum $I^+ + I^-$ being equivalent to scattering of unpolarized neutrons for the Co nanoparticle films with 18 layers (top right) and 3 layers (bottom right). The bright spot images the direct beam and below the horizon at $q_z = 0$, $q_y = 0$ and is surrounded with an extensive halo of small angle scattering in case of the thicker and with a weaker one in case of the thinner nanoparticle film. The specularly reflected beam is seen as a bright spot at $q_z = 0.012$ Å^{-1} and the Yoneda peak at $q_z = 0.006$ Å^{-1} are disposed to the right from the horizon line.

Among the other prominent features displayed in the maps, one can distinguish the scattering intensity concentrated into rings centered around the incident beam and along the vertical line disposed just to the right from the line of low intensity. The latter fixed to the glacing angle of

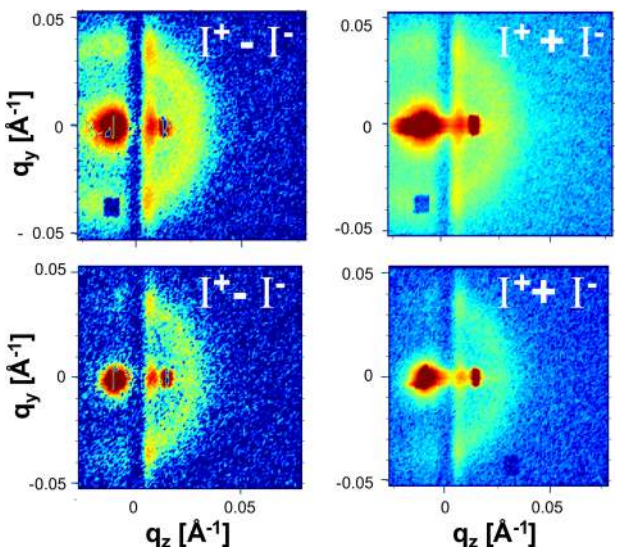

FIG. 4. (Color online) PGISANS data taken with a spin flipper in front of the sample. Difference $(I^+ - I^-)$ between scattering intensities $I^{\pm}$ with alternative polarization (left column) and their sum $(I^+ + I^-)$ (right column). The difference was taken at fields of 110 mT. In the top row measurements from a Co nanoparticle film with 18 layers is shown and in the bottom row measurements from a film with 3 layers. The intensity is plotted in a color code that preferentially works out differences in intensity in a particular intensity range and is based on log-scale.

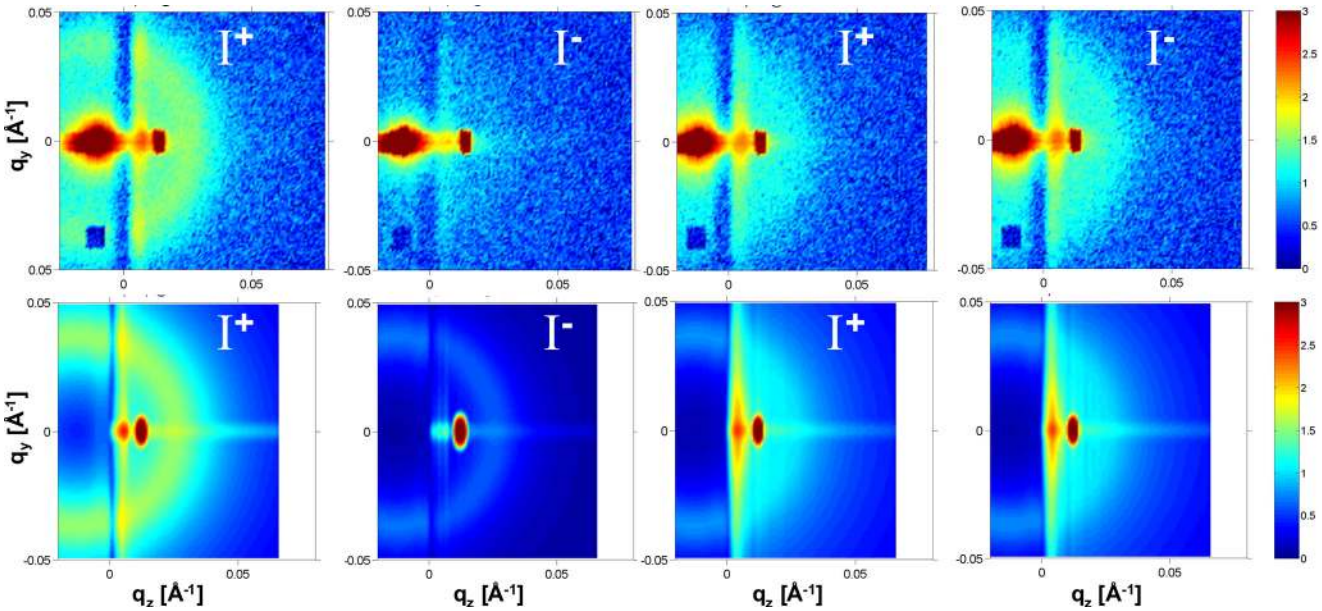

FIG. 5. (Color online) PGISANS data taken with a spin flipper in front of the sample at a film with 18 layers of Co nanoparticles with a diameter of (13.5 ± 1.0) nm (top row) and simulations of the respective PGISANS data (bottom row). The two left columns present data taken at a magnetic field of 110 mT and the right two columns present data taken in remanence. The first and the third column present intensity maps of the up state (I^+) and the second and the fourth column intensity maps of the down state (I^-).The intensity is plotted in a regular color code log-scale.

scattering $\alpha_f = 0$ corresponds to forbidden scattering along the sample surface (sample horizon), while the position of the former one is determined by the critical angle α_c of the total reflection for neutrons scattered at the glancing angle $\alpha_f = \alpha_c$. The scattering intensity strongly varies over the ring and along the vertical line $\alpha_f = \alpha_c$ revealing maxima at the points where this line intersects the ring, or the horizontal line $q_y = 0$. The enhancement of SANS along the line $\alpha_f = \alpha_c$ constitutes the Yoneda effect, which is at the incident angles $\alpha_i \gg \alpha_c$ due to the constructive interference of mainly two different scattered neutron waves. The first one is refracted through the mean optical potential after scattering from nano-particles. The other wave is firstly scattered from nano-particles toward substrate. Then it specularly reflected from the interface with the substrate into the same direction, as the first scattered wave. At the scattering angle $\alpha_f = \alpha_c$ both waves are exactly in-phase.

The well pronounced Debye-Scherrer rings assume short range paracrystalline-type order in the nanoparticle positions within the plane perpendicular to the film surface. Such an arrangement assumes no orientational order over appreciable distances, but a positional order extending over distances longer than in liquids. A quantitative interpretation is based on simulations of the PGISANS data with a program based on the distorted wave Born Approximation (DWBA.) In DWBA all distortions of incoming and scattered neutron waves due to the optical processes, i.e., refraction and reflection, are accounted for exactly, while scattering of those distorted waves from nano-particles is taken in the first Born approximation.

From the simulations of the PGISANS data (see Fig. 5) we gain the following parameters. First, the radius of the Debye-Sherrer ring defines the inter-particle distance that was found to be 17 nm. Short-range correlations are quantified by the width of the Debye-Scherrer ring. From our simulations we infer a very small correlation length of about the inter-particle distance, meaning that over a short length scale Co nanoparticles are densely and almost randomly packed. On the other hand, from our simulations we also conclude that the particle density fluctuates with long-range correlations extended over 400 nm. Those density fluctuations may qualitatively already be recognized in the SEM images.

VI. GISAXS RESULTS ON FE-OXIDE NANOPARTICLES

We have performed GISAXS measurements on the self assembled monolayers of Fe-oxide nanoparticles, the corresponding GISANS measurements will follow in due time. For the GISAXS experiments, we used the beam line ID-10b at the European Sychrotron Radiation Facilitiy (ESRF, Grenoble, France) with a fixed photon energy of 7956 eV and a wavelength of 1.559 Å at a glancing incident angle of 0.2° with a slit width of 30 μm. A CCD camera with pixel size 60 μm and resolution of 0.0095° captured the scattered intensity.

Figure 6 shows the GISAXS pattern for a monolayer (left panel) and a multilayer film (right panel). In both cases we observe pronounced rings of intensity and Bragg peaks centered on these rings. The circles again resemble Debye Scherrer rings from short range positional ordering of the nanoparticles in the $y - z$ plane. On top of these rings we observe Bragg peaks that occur due to the long-range structural ordering in the y-direction. From the width of the Bragg peaks we estimate an average long range order domain size of about 120 nm, which is in very good agreement with the grain size estimated from the SEM pictures. The difference between the monolayer and the multilayer case is that the Bragg peaks in the former case substantially streak out into the z direction, being equivalent to truncation rods in the case of atomic monolayers. This is an indication of the high perfection of the lateral ordering arrangement of the nanoparticles.

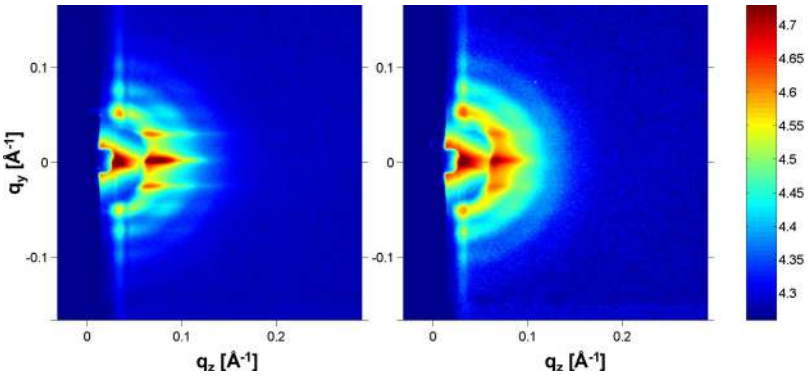

FIG. 6. (Color online) GISAXS patterns from a monolayer of FeO nanoparticles (left) and a multilayer with 4 layers of FO nanoparticles (right). The intensity is plotted in a regular color code log-scale.

VII. SUMMARY

In summary, we have investigated the structural and magnetic properties of self assembled magnetic nanoparticles, in particular of Co- and Fe-oxide nanoparticles ranging from single monolayers up to 18 monolayers. We discussed the differences between simple dropcasting and spin-coating of magnetic nanoparticles. Via spin-coating the surface roughness is reduced leading to a higher reflectivity. We have successfully performed PNR and PGISANS experiments on dropcasted self assembled Co nanoparticle films. Dramatically enhanced sensitivity with respect to the structural organization of the magneto-organic complexes is achieved in our experiment via the spin contrasting of their magnetic core. The PNR scans show well pronounced Kiessig fringes with strong magnetic contrast, while Bragg peaks expected from the periodic layering of the nanoparticle monolayers could not be discerned. The PGISANS maps display well pronounced Debye-Scherrer rings with strong magnetic contrast, indicative for short range lateral order. Again, Bragg reflections from lateral long range magnetic order of the magnetic nanoparticles could not be observed. Quantitative description of the 3 D arrangement of the nanocomposite films is accomplished via fitting of PNR and simulations of the PGISANS data. Simulation of the PNR data revealed that the Co nanoparticles have a diameter of 13.5 nm, which is in good agreement with the results of the TEM measurement. Fe-oxide nanoparticles exhibit superior lateral ordering as compared to the Co-nanoparticles and also the layering is better. GISAXS measurements not only exhibit the Bragg peaks from the lateral order but also show a structural coherence length, which matches very well with the grain size estimated by SEM.

ACKNOWLEDGMENTS

We gratefully acknowledge financial support by the BMBF (O5KN7PC1) and by the ILL. We thank Nadine Mill, and Axel Dreyer for the synthesis of the Co and CoFe nanoparticles, Max Wolff for support at the ADAM reflectometer at ILL, Charles Dewhorst for support at the instrument D22 at the ILL, and Alexei Vorobiev for assistance at the beam line ID-10b at the ESRF.

[1]U. Häfeli, W. Schütt, J. Teller, and M. Zborowski, *Scientific and Clinical Applications of Magnetic Carriers* (Plenum, New York, 1997).
[2]W. S. Seo, J. H. Lee, X. Sun, Y. Suzuki, D. Mann, Z. Liu, M. Terashima, P. C. Yang, M. V. McConnell, D. G. Nishimura, and H. Dai, Nature Mater. **5**, 971 (2006).
[3]P. Oh, P. Borgström, H. Witkiewicz, Y. Li, B. J. Borgström, A. Chrastina, K. Iwata, K. R. Zinn, R. Baldwin, J. E. Testa, and J. E. Schnitzer, Nature Biotechnol. **25**, 327 (2007).
[4]H. Lee, A. M. Purdon, V. Chu, and R. M. Westervelt, Nano Lett. **4**, 995 (2004).
[5]Y. Sun, M. B. Salamon, K. Garnier, and R. S. Averback, Phys. Rev. Lett. **91**, 167206 (2003).
[6]R. Hergt, R. Hiergeist, I. Hilger, W. A. Kaiser, Y. Lapatnikov, S. Margel, and U. Richter, J. Magn. Magn. Mater. **270**, 345 (2004).
[7]R. Hergt, S. Dutz, R. Müller, and M. Zeisberger, J. Phys.: Condens. Mat. **18**, S2919 (2006).
[8]C. B. Murray, S. Sun, W. Gaschler, H. Doyle, T. A. Betley, and C. R. Kagan, IBM J. Res. Dev. **45**, 47 (2001).
[9]V. F. Puntes, K. M. Krishnan, and A. P. Alivisatos, Science **291**, 2115 (2001).
[10]D. P. Dinega and M. G. Bawendi, Angew. Chem. **111**, 1906 (2001).
[11]S. Sun, C. B. Murray, D. Weller, L. Folks, and A. Moser, Science **287**, 1989 (2000).
[12]A. L. Rogach, D. V. Talapin, E. V. Shevchenko, A. Kornowski, M. Haase, and H. Weller, Adv. Funct. Mater. **12**, 653 (2002).
[13]E. L. Bizdoaca, M. Spasova, M. Farle, M. Hilgendorff, L. M. Liz-Marzan, and F. Caruso, J. Vac. Sci. Technol. A **21**, 1515 (2003).
[14]C. Nayral, E. Viala, P. Fau, F. Senocq, J.-C. Jumas, A. Maisonnat, and B. Chaudret, Chemi. - A Eur. J. **6**, 4082 (2000).
[15]A. K. Gupta1 and A. S. G. Curtis, J. Mater. Sci.: Mater. Med. **15**, 493 (2004).
[16]B. P. Toperverg, in *Polarized Neutron Scattering, Series Matter and Materials*, Jülich Series "Matter and Materials" edited by T. Brückel and W. Schweika (Forschungszentrum Juelich GmbH, Institut für Festkörperforschung: Germany 2002), p. 249, Vol. 12.
[17]H. Zabel, K. Theis-Bröhl, and B. Toperverg, "Polarized neutron reflectivity and scattering of magnetic nanostructures and spintronic materials", in *Handbook of Magnetism and Advanced Magnetic Materials*, edited by H. Kronmüller and S. Parkin (Wiley, New York, 2007), p. 1237.
[18]A. Schreyer, R. Siebrecht, U. English, U. Pietsch, and H. Zabel, Physica B **248**, 349 (1998).
[19]M. Wolff, K. Zhernenkov, and H. Zabel, Thin Solid Films **515**, 5712 (2007).
[20]A. Hütten, D. Sudfeld, I. Ennen, G. Reiss, W. Hachmann, U. Heinzmann, K. Wojczykowski, P. Jutzi, W Saikaly, and G Thomas, J. Biotechnol. **112**, 47 (2004).
[21]P. Kumar, Nanoscale Res. Lett. **5**, 1367 (2010).
[22]Y.-K. Hong, H. Kim, G. Lee, W. Kim, and J.-Y. Koo, Appl. Phys. Lett. **80**, 844 (2002).
[23]The package uses the super-iterative algorithm.
[24]With a magnetization of 96% of the saturation magnetization.
[25]The intensity maps are plotted in coordinates q_y and q'_z, the Cartesian projections of the wave vector transfer **q**. The y axis of the coordinate system is perpendicular to the specular reflection plane, while the z'-axis lies within this plane and is directed perpendicular to the incident beam (x'-axis). So the z'-axis is tilted by a small incidence angle against the sample normal traditionally chosen in reflectometry as the z-axis.